ELSEVIER

Journal of Alloys and Compounds 243 (1996) 126–132

Journal of
ALLOYS
AND COMPOUNDS

The oxidation behavior of Ni$_3$Al–Zr alloys with various zirconium contents

T.T. Chang[a], Y.C. Pan[b], T.H. Chuang[a,*]

[a] *Institute of Materials Science and Engineering, National Taiwan University, Taipei, Taiwan*
[b] *Chung Shan Institute of Science and Technology, Taoyuan, Taiwan*

Received 2 March 1996; in final form 24 April 1996

Abstract

The oxidation behavior of Ni$_3$Al alloys with zirconium additions was studied after long-term air exposure over a temperature range of 560–1300°C. The results showed that the penetration of oxides into Ni$_3$Al–Zr alloys along the grain boundaries was caused by the formation of ZrO$_2$. The penetration depth of the oxides increased with an increase of the zirconium content and oxidation temperature. The reaction of the oxides was controlled by oxygen diffusion in allotropic ZrO$_2$, and the lines in the Arrhenius diagram of the reaction rate constants reflected at 1050°C. However, the penetration of oxides was not seen in the alloy without zirconium addition. Through electron probe microanalysis and X-ray diffraction, the compositions and structures of the oxides for these alloys were also determined.

Keywords: Ni$_3$Al intermetallic compound; Oxidation; Penetration oxide

1. Introduction

The Ni$_3$Al intermetallic compound possesses a high melting point and high strength. The yield strength has been shown to increase with increasing temperature [1]. Since Ni$_3$Al has the advantages of lower density and lower cost for raw materials compared with commercial superalloys, it is a promising substitute for them. However, there exists a major problem of brittle intergranular fracture in polycrystalline Ni$_3$Al [2–4]. Aoki and Izumi [5] first reported that the brittleness of Ni$_3$Al could be minimized by adding trace amounts of boron. Liu et al. [3] showed that room temperature elongation of Ni$_3$Al could be increased to 50% by controlling the addition of boron, the alloy stoichiometry and the thermomechanical treatment.

In the development of Ni$_3$Al alloys, zirconium addition has been shown to improve high-temperature strength and creep resistance [6]. For engineering applications, the effect of zirconium addition on the oxidation behavior of this alloy should be considered. Taniguchi and coworkers [7,8] indicated that zirconium could form a very adherent oxide scale on the cyclic oxidation and isothermal oxidation behavior of Ni$_3$Al–0.1B base containing titanium, zirconium or hafnium addition. Pandey et al. [9] studied the effect of zirconium on the cyclic oxidation behavior of Fe–15Cr–4Al alloy at 1300°C, and their results show that addition of 0.2% zirconium to the base alloy suppresses nodule formation and provides the best resistance to cyclic oxidation. Barrett [10] indicated that small amounts of added zirconium dramatically increase the cyclic oxidation resistance of β-NiAl by minimizing Al$_2$O$_3$ spalling during the cooling cycles, and scale-spall resistance was associated with small amounts of ZrO$_2$ in the Al$_2$O$_3$ scale. Rybicki and Smialek [11] observed a discontinuous decrease in the growth rate of two orders of magnitude at 1000°C due to the formation of α-Al$_2$O$_3$ from θ-Al$_2$O$_3$ on the isothermal oxidation of NiAl + Zr, which was performed over a temperature range of 800–1200°C. Smialek et al. [12] showed that the parabolic growth rates for the FeAl + Hf,Zr,B alloys were about five times higher than those for the NiAl + 0.1Zr alloy. Taniguchi et al. [13] indicated that the addition of zirconium to Fe–23Cr–5Al resulted in very adherent Al$_2$O$_3$ scales after preoxidation, which did not increase the protection time of sulfidation because the ZrO$_2$ particles in the scale

---

[*] Corresponding author.

PII S0925-8388(96)02370-5

provided sites for preferential sulfide formation. In a previous work [14], the penetration of oxides along the grain boundaries was seen in the Ni_3Al–1 at.% Zr alloys with or without chromium addition after oxidation tests. The present paper shows further that the penetration depth of oxides in the Ni_3Al–Zr alloys depends on the zirconium content and the oxidation temperature after air exposure in a temperature range from 560 to 1300°C.

2. Experimental procedure

The Ni_3Al–Zr alloys in the present study were melted to produce $25 \times 100 \times 80$ mm^3 ingots from Ni and Al of 99.9 pct. purity, and Ni–B and Ni–Zr master alloys in a vacuum induction furnace. Table 1 shows the chemical compositions of the Ni_3Al–Zr alloys studied. Chemical analysis showed that the oxygen and carbon contents in these alloys were below 70 ppm, and that the residual hydrogen content was less than 10 ppm. The boron concentrations for various Ni_3Al–Zr alloys were 500 ± 10 ppm. The ingots were cut into 6 mm thick plates and thermomechanically treated repeatedly by cold rolling and annealing in an air furnace in a temperature range from 1100 to 1000°C for 1 h. After the thermomechanical treatment, the sheets had a final thickness of 1.2 mm, and were then sliced into 10×20 mm^2 specimens for oxidation tests.

All the specimens were polished to 1200 grit and ultrasonically cleaned with acetone. The oxidation tests were conducted in an air furnace at various temperatures between 560 and 1300°C with exposure periods ranging from 0.5 to 480 h. The cross-sections of the oxidized specimens were observed using optical and scanning electron microscopy. The composition of the oxide scale was analyzed by means of an electron probe for microanalysis (EPMA). Structural identification of the oxides was performed by using an X-ray diffractometer (XRD). The penetration depths of the oxides were measured from the surface to the front of the oxides by means of optical microscopy; 50 values were obtained to yield the average penetration depth.

Table 1
Chemical compositions of the Ni_3Al–Zr alloys studied

Alloy	Ni (wt.%)	Al (wt.%)	Zr (wt.%)	B (wt.%)
$Ni_{78}Al_{22}$	bal.	11.48	–	0.05
$Ni_{78}Al_{21.7}Zr_{0.3}$	bal.	11.28	0.53	0.05
$Ni_{78}Al_{21.4}Zr_{0.6}$	bal.	11.08	1.05	0.05
$Ni_{78}Al_{21.2}Zr_{0.8}$	bal.	10.95	1.40	0.05
$Ni_{78}Al_{21}Zr_1$	bal.	10.82	1.74	0.05
$Ni_{78}Al_{20.5}Zr_{1.5}$	bal.	10.50	2.60	0.05
$Ni_{78}Al_{20}Zr_2$	bal.	10.18	3.44	0.05

3. Results and discussion

The cross-sections of the Ni_3Al alloys containing 0–2 at.% zirconium after air exposure at 1150°C for 72 h are shown in Figs. 1(a)–1(g). It can be seen that the oxidation products of the zirconium containing alloys penetrated along the grain boundaries into the material interior, and that the penetration oxides then

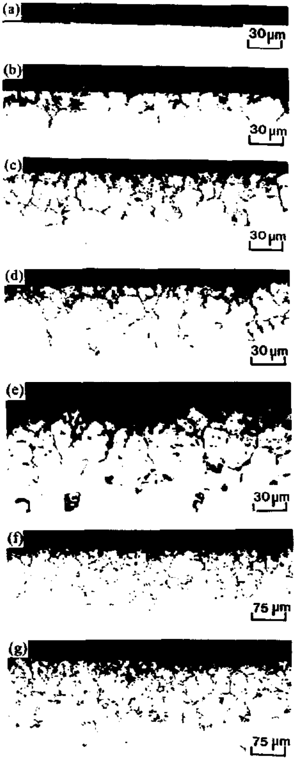

Fig. 1. The cross-sections of the Ni_3Al alloys containing (a) 0%, (b) 0.3%, (c) 0.6%, (d) 0.8%, (e) 1%, (f) 1.5% and (g) 2% zirconium after air exposure at 1150°C for 72 h.

interlocked with the matrix to form an adherent oxide scale. The penetration depths of the oxides increased with an increase of the zirconium content, as shown in Fig. 2. However, penetration of oxides was not seen in the alloy without zirconium addition.

Figs. 3(a)–3(g) show the cross-sections of the Ni$_{78}$Al$_{20}$Zr$_2$ alloy after oxidation tests at different oxidizing temperatures between 560 and 1300°C. It can be seen that a continuous oxide film formed on the outer surface at all the temperatures. The oxidation products also penetrated along the grain boundaries into the matrix of the material, and the penetration depth of the oxides increased with an increase of the oxidation temperature, as shown in Fig. 4.

The values obtained by squaring the penetration depths of these oxidation products divided by the exposure time, which correspond to the square of the reaction rate constants, are shown in Table 2. The reaction rate constant increased with increasing zirconium content, as shown in Fig. 5. The values obtained by squaring the reaction rate constants of Table 2 are also plotted in an Arrhenius diagram in Fig. 6, which shows that a linear relationship exists for these alloys. This implies that the reaction was diffusion controlled, which is primarily attributable to the diffusion of oxygen in ZrO$_2$. However, there is an inflection in these lines at 1050°C. The activation energies of these alloys above and below 1050°C were calculated from Fig. 6 and are shown in Table 3. Since ZrO$_2$ possesses a tetragonal structure above 1050°C and a monoclinic structure below 1050°C, the inflection might be caused by oxygen diffusion in different crystal structures above and below 1050°C. Ando et al. [15] showed that the activation energy for oxygen self-diffusion in tetragonal 14 mol% CeO$_2$–86 mol% ZrO$_2$ was 355.3 kJ mol^{-1} (84.6 kcal mol^{-1}). In addition, the activation energy for oxygen lattice-diffusion

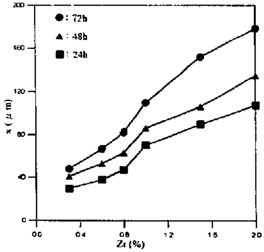

Fig. 2. The penetration depth of the oxides (x) versus the zirconium content (Zr%) for Ni$_3$Al–Zr alloys at 1150°C for 24, 48 and 72 h.

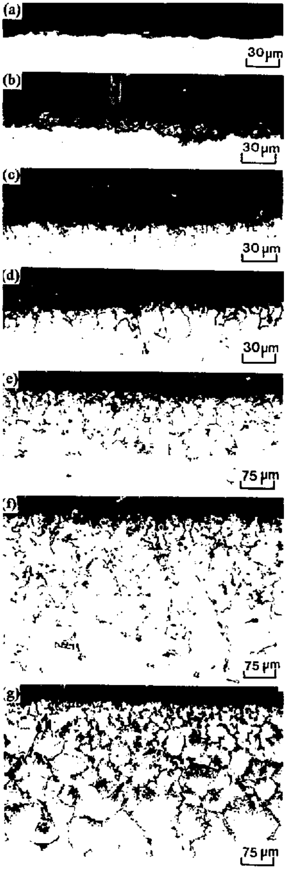

Fig. 3. The cross-sections of the Ni$_{78}$Al$_{20}$Zr$_2$ alloy after air exposure at various temperatures: (a) 560°C, 480 h; (b) 850°C, 360 h; (c) 950°C, 288 h; (d) 1050°C, 192 h; (e) 1150°C, 72 h; (f) 1200°C, 48 h and (g) 1300°C, 4 h.

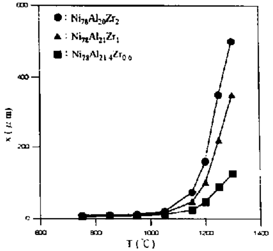

Fig. 4. The penetration depth of the oxides (x) versus the oxidation temperature T for Ni_3Al–Zr alloys over 12 h.

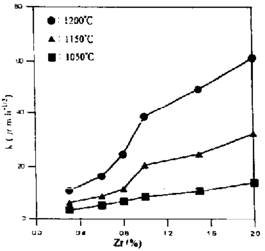

Fig. 5. The reaction rate constant k versus the zirconium content (Zr%) for the Ni_3Al–Zr alloys at different oxidation temperatures.

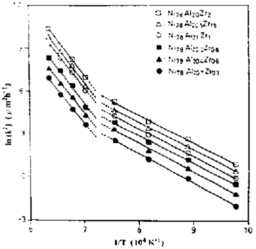

Fig. 6. Arrhenius diagrams of the square of the reaction rate constants for the Ni_3Al–Zr alloys with various zirconium contents.

in monoclinic ZrO_2 was found by Ikuma et al. [16] to be 87.0 kJ mol^{-1} (20.7 kcal mol^{-1}). From our results, the activation energy of oxygen diffusion in tetragonal ZrO_2 is larger than that in monoclinic ZrO_2, which is consistent with the change of slope in the linear reflection of Fig. 6 above and below 1050°C.

Figs. 7(a)–7(e) are the elemental distribution of the $Ni_{78}Al_{20}Zr_2$ alloy after air exposure at 1150°C for 24 h. It can be seen that the external scale consists of an outer layer rich in nickel, which was NiO, and an inner layer rich in aluminum and zirconium, which was Al_2O_3 and ZrO_2, and that the ZrO_2 was incorporated into the Al_2O_3 layer. The inner layer extended further into the matrix to form the penetration oxides. Thus, the Al distribution of the penetration oxides fell behind the Zr distribution of the penetration oxides. Likewise, the front of the penetration oxides was only rich in zirconium. When the oxide scale formed, the oxygen partial pressure decreased. However, the oxygen first tended to react with the zirconium, which was a strongly active element. Then, the oxygen again diffused through the oxides and reacted with aluminum to form Al_2O_3. Fig. 8 is a light-etching micrograph of the $Ni_{78}Al_{20}Zr_2$ alloy after air exposure at 1150°C for 24 h. It shows the depletion of the zirconium region and an irregular interface around the oxides which penetrated along the grain boundaries. Figs. 9(a) and 9(b) are the EDX spectra obtained from the de-zirconium region and the interior of the matrix. It shows that the penetration oxides consumed the zirconium and left the region depleted of zirconium around the penetration oxides. Also, the Al intensity of the region was less than that of the matrix shown in Fig. 9.

The XRD spectra for the oxide film of the $Ni_{78}Al_{22}$

Table 2
The reaction rate constants k(μm h$^{-1/2}$) of the penetration oxides for the Ni_3Al–Zr alloys

T (°C)	$Ni_{78}Al_{21.7}Zr_{0.3}$	$Ni_{78}Al_{21.4}Zr_{0.6}$	$Ni_{78}Al_{21.2}Zr_{0.8}$	$Ni_{78}Al_{21}Zr_1$	$Ni_{78}Al_{20.5}Zr_{1.5}$	$Ni_{78}Al_{20}Zr_2$
1300	31.37	44.33	63.73	105.54	131.90	175.16
1250	17.69	26.48	40.77	64.34	80.10	99.67
1200	10.89	16.32	24.45	38.63	49.41	61.31
1150	6.29	8.83	11.64	20.67	24.64	32.21
1050	3.51	5.43	6.86	8.49	10.81	14.05
950	1.82	2.50	3.37	4.39	5.67	7.01
850	0.94	1.36	1.79	2.30	2.92	3.77
750	0.36	0.56	0.77	0.96	1.24	1.55

Table 3
The activation energy of the penetration oxides for the Ni_3Al–Zr alloys

Alloy	Activation energy (kcal mol^{-1})	
	$T < 1050$ °C	$T > 1050$ °C
$Ni_{78}Al_{21.7}Zr_{0.3}$	40.2	94.3
$Ni_{78}Al_{21.4}Zr_{0.6}$	39.9	95.0
$Ni_{78}Al_{21.2}Zr_{0.8}$	38.6	94.8
$Ni_{78}Al_{21}Zr_{1}$	39.0	96.2
$Ni_{78}Al_{20.5}Zr_{1.5}$	38.5	98.3
$Ni_{78}Al_{20}Zr_{2}$	38.9	99.1

alloy are shown in Fig. 10. Only the NiO peaks can be found after air exposure at 750°C for 432 h (Fig. 10(a)). With an increase of the exposure temperature to 1050°C (Fig. 10(b)), the XRD patterns show peaks of NiO, $NiAl_2O_4$ and Al_2O_3. With an increase of the exposure temperature, the intensity of the $NiAl_2O_4$ and Al_2O_3 peaks increases, and the intensity of the NiO peaks decreases (Fig. 10(c)). Because the inner Al_2O_3 film reacts with the outer NiO film to form an intermediate $NiAl_2O_4$ layer at high temperatures, the intensity of the NiO peaks decreased.

Fig. 8. The cross-section of the $Ni_{78}Al_{20}Zr_2$ alloy after air exposure at 1150°C for 24 h.

Fig. 11 shows the XRD spectra for the oxide film of the $Ni_{78}Al_{20}Zr_2$ alloy after the oxidation tests. In addition to peaks similar to those in Fig. 10 for $Ni_{78}Al_{22}$, the peaks of ZrO_2 can be observed in the

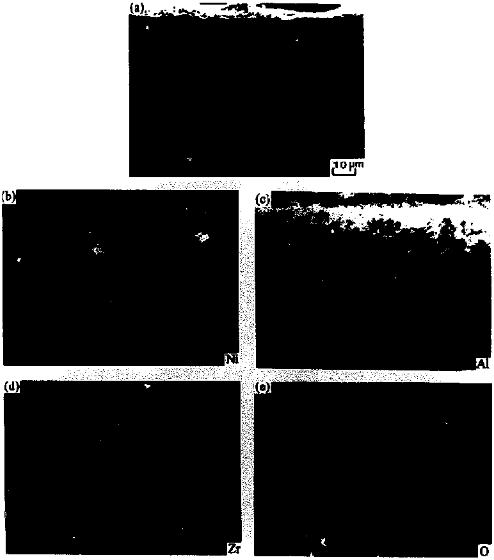

Fig. 7. The distribution of elements of the $Ni_{78}Al_{20}Zr_2$ alloy determined by EPMA after air exposure at 1150°C for 24 h: (a) the secondary electron image, (b) nickel, (c) aluminum, (d) zirconium and (e) oxygen.

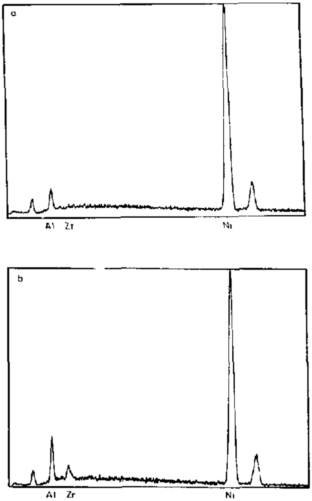

Fig. 9. EDX spectra obtained from (a) the de-zirconium region and (b) the interior of the matrix as shown in Fig. 8.

alloys with zirconium addition. The intensity of NiO peaks is also strong for the alloy after air exposure at 750°C for 432 h. Each peak of ZrO_2 and $NiAl_2O_4$ can also be seen in Fig. 11(a). With an increase of the exposure temperature to 1050°C, the peaks for NiO, ZrO_2, $NiAl_2O_4$ and Al_2O_3 are as shown in Fig. 11(b). The intensity of the $NiAl_2O_4$, Al_2O_3 and ZrO_2 peaks increased with increasing exposure temperature.

Fig. 12 shows XRD spectra for the oxide film of the alloys containing 0, 0.6 and 2 at.% zirconium after air exposure at 1050°C for 100 h. The intensity of the NiO, ZrO_2, $NiAl_2O_4$ and Al_2O_3 oxide peaks increased with increasing zirconium addition.

Summarizing the results of the morphological observations and chemical analyses, the penetration oxides along the grain boundaries were due to the formation of the ZrO_2 [14]. Oxygen diffused through the outer oxide layers to the interface of the penetration oxides and reacted with zirconium, which diffused along the shortest path (the grain boundaries) to the interface to form the intergranular ZrO_2, and this exhausted the zirconium and left a de-zirconium region. It was confirmed that zirconium was distributed in front of the penetration oxides. With an increase

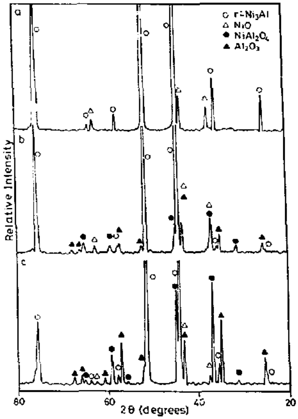

Fig. 10. XRD spectra of the oxide scales for the $Ni_{78}Al_{22}$ alloy after air exposure at various temperatures: (a) 750°C, 432 h; (b) 1050°C, 100 h and (c) 1200°C, 48 h.

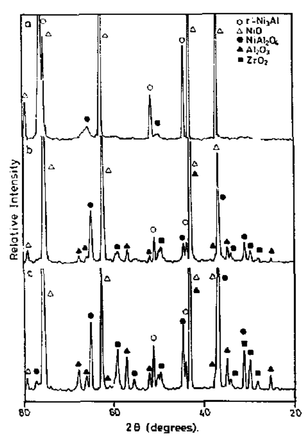

Fig. 11. XRD spectra of the oxide scales for the $Ni_{78}Al_{20}Zr_2$ alloy after air exposure at various temperatures: (a) 750°C, 432 h; (b) 1050°C, 100 h and (c) 1200°C, 48 h.

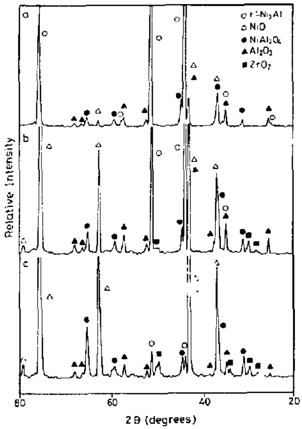

Fig. 12. XRD spectra of the oxide scales for the Ni_3Al alloys containing (a) 0%, (b) 0.6% and (c) 2% zirconium after air exposure at 1050°C for 100 h.

of the zirconium content, the penetration depth of the oxides increased. For engineering applications, decreasing the zirconium content could decrease the penetration depth of the oxides and result in an adherent oxide scale, maintaining the scale-spall resistance.

4. Conclusions

The oxides which formed on the Ni_3Al–Zr alloys penetrated along the grain boundaries into the matrix. This was caused by the formation of ZrO_2, which could interlock with the matrix to form an adherent oxide scale. In the Ni_3Al alloy without zirconium addition, penetration of oxides could not be seen. With an increase of the zirconium content and the oxidation temperature, the penetration depth of the oxides increased. The reaction of the penetration oxides was diffusion-controlled, due to the oxygen diffusion in ZrO_2. An inflection point (1050°C) for the Arrhenius diagram of the square of the reaction rate constant was caused by the oxygen diffusion in monoclinic ZrO_2 below 1050°C and in tetragonal ZrO_2 above 1050°C. The zirconium addition assisted the formation of an oxide layer in the Ni_3Al alloys. Thus, the intensities of the NiO, $NiAl_2O_4$, Al_2O_3 and ZrO_2 peaks increased with an increase of the zirconium content in the XRD spectra.

References

[1] O. Noguchi, Y. Oya and T. Suzuki, *Metall. Trans.*, *12A* (1981) 1647.
[2] T. Ogura, S. Hanada, T. Masumoto and O. Izumi, *Metall. Trans.*, *16A* (1985) 441.
[3] C.T. Liu, C.L. White and J.A. Horton, *Acta Metall.*, *33* (1985) 213.
[4] T. Takasugi, E.P. George, D.P. Pope and O. Izumi, *Scripta Metall.*, *19* (1985) 551.
[5] K. Aoki and O. Izumi, *J. Jpn. Inst. Met.*, *43* (1979) 1190.
[6] S.E. Hsu, N.N. Hsu, C.H. Tong, P.H. Hu and J.Y. Ma, in *Proc. Ann. Conf. Chin. Soc. Mater. Sci.*, *1986*, p. 423.
[7] S. Taniguchi and T. Shibata, *Oxid. Met.*, *25* (1986) 201.
[8] S. Taniguchi, T. Shibata and H. Tsuruoko, *Oxid. Met.*, *26* (1986) 1.
[9] J.L. Pandey, S. Prakash and M.L. Mehta, *Oxid. Met.*, *29* (1988) 1.
[10] C.A. Barrett, *Oxid. Met.*, *30* (1988) 361.
[11] G.C. Rybicki and J.L. Smialek, *Oxid. Met.*, *31* (1989) 275.
[12] J.L. Smialek, J. Doychak and D.J. Gaydosh, *Oxid. Met.*, *34* (1990) 259.
[13] S. Taniguchi, T. Shibata and H. Tsuruoka, *Oxid. Met.*, *32* (1989) 391.
[14] Y.C. Pan and T.H. Chuang, *J. Mater. Sci.*, *26* (1991) 6097.
[15] K. Ando, S. Morita and R. Watanable, *Yogyo Kyokaishi*, *94*(8) (1986) 732.
[16] Y. Ikuma, K. Komatsu and W. Komatsu, in S. Somiya, N.Y. Amamoto and H. Yanagida (eds.), *Advances in Ceramics Vol. 24B, Science and Technology of Zirconia III*, American Ceramic Society, Westerville, OH, 1988, p. 749.